Unsupervised Recognition of Retinal Vascular Junction Points

Luigi Di Rosa [a], Hadi Hamad [b,c], Domenico Tegolo [c], Cesare Valenti [c]
[a] Clinica Oculistica, Policlinico Universitario, Palermo, Italy
[b] Department of Mathematics, An-Najah National University, Palestine
[c] Dipartimento di Matematica e Informatica, Università degli Studi di Palermo, Italy
hadihamad@najah.edu, domenico.tegolo@unipa.it, cesare.valenti@unipa.it

***Abstract*— Landmark points in retinal images can be used to create a graph representation to understand and to diagnose not only different pathologies of the eye, but also a variety of more general diseases. Aim of this paper is the description of a non-supervised methodology to distinguish between bifurcations and crossings of the retinal vessels, which can be used in differentiating between arteries and veins. A thinned representation of the binarized image, is used to identify pixels with three or more neighbors. Junction points are classified into bifurcations or crossovers according to their geometrical and topological properties. The proposed approach is successfully compared with the state-of-the-art methods with the benchmarks DRIVE and STARE. The recall, precision and F-score average detection values are 91.5%, 88.8% and 89.8% respectively.**

I. Introduction

Retinal image analysis is particularly useful because it is a non-invasive repeatable diagnostic practice to highlight both pathologies of the eye and other diseases (e.g. diabetic retinopathy and hypertension) which modify the caliper of arteries or lead to new vessels and branches [1]. Since the definition of a standard and automatic way to quantify morphometric features of the retinal vessels is desirable, a number of academics worked on retinal image segmentation. Self-organizing feature maps [2] have been adopted to model implicit cost functions for the junction geometry, and the network connectivity is identified by resolving the configuration of local sets of segment ends. A two-steps approach is defined in [3]: the former applies imaging techniques (mainly filters and morphologic operations) to obtain the base structure for vessels detection; the latter classifies crossover or bifurcation by analyzing the feature point's environment. Recently, a local operator, applied to the centerline of the already thinned segmentation, was presented in [1].

In the last decade two main techniques were designed to locate the vascular landmarks, based on geometrical-features (as in our approach) which require some kind of image manipulation or are based on models which cannot be generalized easily. For example, a training phase is used to configure a bank of Gabor filters to identify the landmark points, but not to distinguish between bifurcations and crossovers [4]. The Kalman filter is applied depending on the continuities in curvature, width and intensity changes at the bifurcation and the crossing points to identify the vascular tree and a minimum-cost matching algorithm resolves eventual tracing errors [5]. A hybrid approach detected the bifurcation and intersection points in the fundus images using a window of 5×5 pixels [6]. An automatic approach to classify arteries and veins was proposed in [7]: a graph representation of their centerlines, extracted from the segmented image, is used in order to classify the landmarks.

We already developed methodologies to automatically segment retinal images by using AdaBoost [8] and Fuzzy C-Means clustering [9]. The method proposed here introduces a new technique which uses the graph representation of the segmented images and further features round the junction points to achieve a better reliable classification performance.

This work was supported partially by grant CUP B71J12001380001, University of Palermo FFR 2012/2013.

II. Material

The forty photographs which constitute the DRIVE dataset were obtained in occasion of a diabetic retinopathy screening program in The Netherlands. Each image has 565×584 pixels and is stored with 8 bits per channel of the RGB color space. The set is divided into training and test subsets with 20 images each, together with corresponding manual binary segmentations [10]. Analogously, the STARE [11] dataset contains 20 retinal images with 700×605 pixels, 8 bits per color channel with manual segmentations. We chose both these datasets as a lot of previous and current works are using them [1], [4], thus a reliable comparison between our method and those by other researchers can be carried out.

III. Methodology

The methodology of the study is divided into two phases: preprocessing and classification. The binary segmented image is analyzed to specify junctions, widths and directions. Each junction is therefore categorized as a bifurcation or a crossover, according to its features.

A. Preprocessing phase

A binary segmentation, is the starting point for the preprocessing stage. Thinning of the segmented images [12], [13] was adopted in this contribution instead of skeletonization, owing to the fact that the thinned image presents smoother segments and contains less spikes which may lead to a false impression about branches and cusps.

The eventual presence of very small sets of black pixels in the low resolution segmented images produces wrong edges which are not in the original input image; we contemplate this case by applying the following rules, in order:

978-1-4244-7929-0/14/$26.00 ©2014 IEEE

- for weakly-connected two components with each less than 200 black pixels, this connection is converted to a strong one by introducing a black pixel (Fig. 1);
- in a weakly connected black pixel to a component with more than 1000 black pixels, this pixel is labeled as foreground (vessel);
- all strongly connected one or two black pixels components must be assigned as foreground.

Fig. 1. Original (left) and enhanced (right) images with their thinnings.

The resulting thinned version represents a graph of the vascular network [14], where each arc is connected at most to two nodes and each node is connected at least to three arcs. Let us define a *vertex* as a pixel connected at least to three components; a *bifurcation* as a vertex connected to exactly three components; a *direct crossing* as a vertex which has four connected components. Wide segments crossing each other usually share an edge in addition to four outer segments (Fig. 2a). We called this type of crossing as a *non-direct crossing* if the length of the common edge is less than 25 pixels. In order to distinguish between these two types of crossings we consider the minimum rectangle that includes the vertices, expanded by one pixel in all directions (Fig. 2):

Direction of the vessels. Various algorithms were described to calculate the local slope of the vessels [1], [2], [7]. We experimentally verified that the *singular value decomposition* on the thinned representation returns appropriate results.

Width of the vessels. Instead of time consuming approaches [1], [15] and due to the low resolution of the images in both datasets, approximated widths of the vessels are sufficient: we count the pixels common to the segment and the perpendicular line of each pixel of the centerline [16]. In the case of less than 7 pixels, a rotational technique is employed [17]. Twelve straight lines each spaced 15 degrees from the next one are positioned around the considered centerline pixel: the minimum number of pixels common in each line is considered as the width of the segment.

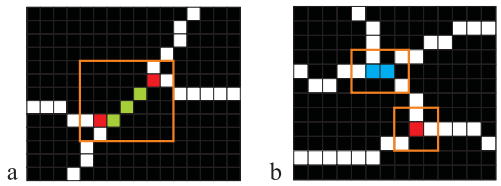

Fig. 2. Enlarged rectangles including vertices with thinned vessels: possible non-direct crossing (a) and direct crossing together with bifurcation (b).

B. Classification phase

To confirm or reject each candidate crossing we consider the features computed during the preprocessing phase.

Identification of direct crossings. A simple yet effective Gestalt approach is applied: two continuing segments generally have nearly equal widths and opposite directions.

- *Width restrictions.*
  Given two pairs of opposite segments for a putative direct crossing (Fig. 3a), let us indicate by w_1, w_3 and w_2, w_4 their widths. Both these conditions, empirically determined, must hold:

$$\begin{cases} \min\left\{\frac{\min\{w_1,w_3\}}{\max\{w_1,w_3\}}, \frac{\min\{w_2,w_4\}}{\max\{w_2,w_4\}}\right\} < 0.15 \\ \max\{|w_1 - w_3|, |w_2 - w_4|\} < 6.2 \end{cases}$$

- *Direction restrictions.*
  Without loss of generality, let us consider $\alpha_1 \leq \alpha_2$, $\beta_1 \leq \beta_2$ and $\alpha_1 + \alpha_2 \leq \beta_1 + \beta_2$. Both angular conditions, empirically determined, must hold:

$$\begin{cases} 0 \leq \alpha_1 \leq \alpha_2 \leq 173^\circ \\ 35^\circ \leq \beta_1 \leq \beta_2 \leq 180^\circ \end{cases}$$

Identification of non-direct crossings. All candidate non-direct crossings are sorted in ascending order with respect to the length of their edges. Starting from the shortest edge, our procedure tests the following criteria, which are analogous to the cases described for direct crossings (Fig. 3b).

- *Width restrictions.*

$$\begin{cases} \min\left\{\frac{\min\{w_1,w_3\}}{\max\{w_1,w_3\}}, \frac{\min\{w_2,w_4\}}{\max\{w_2,w_4\}}\right\} < 0.25 \\ \max\{|w_1 - w_3|, |w_2 - w_4|\} < 3.0 \end{cases}$$

- *Direction restrictions.*

$$\begin{cases} 0 \leq \alpha_1 \leq \alpha_2 \leq 166^\circ \\ \alpha_1 + \alpha_2 \leq 260^\circ \\ \alpha_2 - \alpha_1 \leq 135^\circ \\ \beta_2 - \beta_1 \leq 113^\circ \end{cases}$$

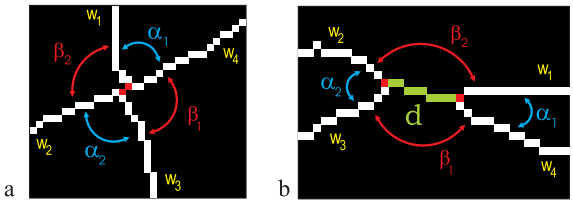

Fig. 3. Example of direct (a) and non-direct crossings (b).

IV. Results and Conclusions

To verify the effectiveness of our methodology, we compared its results against the ground truth manually provided by an expert ophthalmologist, in terms of true positives (TP), false positives (FP) and false negatives (FN). Moreover, the *F-score* was used to evaluate quantitatively the overall accuracy: $F = \frac{2 \times RE \times PR}{RE + PR}$. This measure corresponds to the harmonic mean of the values precision $PR = \frac{TP}{TP+FP}$ and recall $RE = \frac{TP}{TP+FN}$, which reflect respectively the rate of true positive to all positive results and the ability of the

algorithm to detect the landmarks. Correctness (CO) was defined as the average of precision and recall.

The proposed unsupervised approach was fine-tuned on the training images and validated on the test images of both DRIVE and STARE datasets, using their manual segmentation to identify the structural components of the vascular tree outside the optic disk which is considered unreliable [7] and can be located by using the Harris detector [18], [19]. We want to highlight that our method took into consideration all vessels without excluding the smallest ones. Table I reports detailed results for each image (ID), including the number of landmark points obtained by the experts (GT) and by the proposed method in addition to the considered metrics.

Fig. 4 shows that most classifications exhibit a value of at least 80% for PR and RE measurements. We observed a difference in the classification ability among images which show actual pathologies and the quality of their respective segmentations. This difference can be explained by considering the unusual vessel structures. We compared our results with state-of-the-art works, showing better overall recall and precision for both bifurcations and crossings (Fig. 5). The average recall value for bifurcations and crossings detection in the DRIVE and STARE datasets is 91.5%, the average precision value is 88.8%, while the overall bifurcation and crossing F-score values are 90.9% and 88.8% respectively.

Landmark points can be used to control the evolution of diseases and the effectiveness of treatments, after registering photographs acquired at different times [14]. Accurate registration algorithms usually require uniformly distributed points. We plan to include descriptors [20] to locate additional points not necessarily related to the structure of the vessels on the retina. We will investigate also the application of consolidated techniques [21], [22] to enhance the images (e.g. noise reduction and normalization of brightness and saturation). Further experiments should consider high resolution photographs [23] to lessen any artifact due to vessel with calibers comparable to the size of the pixels themselves.

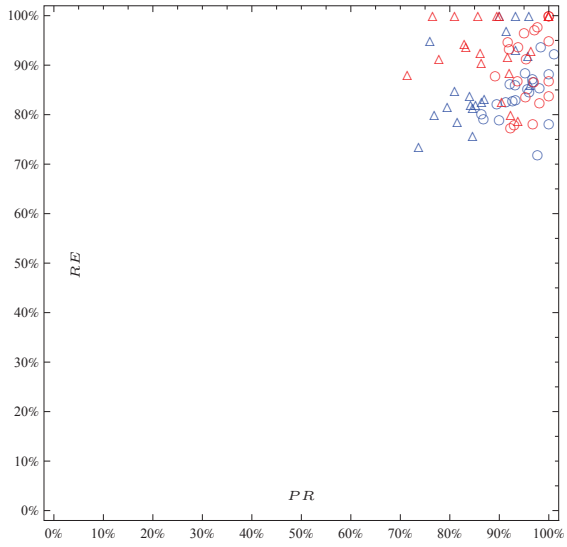

Fig. 4. Precision vs recall for the DRIVE (blue) and STARE (red) datasets. Bifurcations and crossings are represented by triangles and circles.

TABLE I

BIFURCATIONS AND CROSSINGS FOR DRIVE AND STARE DATASETS. THE HIGHLIGHTED IMAGE IS SHOWN IN FIG. 6.

Bifurcations													
	DRIVE dataset						STARE dataset						
ID	GT	Method	TP	FN	FP	F	ID	GT	Method	TP	FN	FP	F
1	104	115	95	9	20	86.8	1	60	59	57	3	2	95.8
2	120	135	112	8	23	87.8	2	52	62	51	1	11	89.5
3	115	129	110	5	19	90.2	3	44	44	43	1	1	97.7
4	124	139	115	9	24	87.4	4	38	40	38	0	2	97.4
5	151	161	139	12	22	89.1	5	65	65	61	4	4	93.9
6	146	158	136	10	22	89.5	44	34	34	33	1	1	97.1
7	125	135	114	11	21	87.7	77	65	68	62	3	6	93.2
8	99	111	90	9	21	85.7	81	60	58	55	5	3	93.2
9	110	123	108	2	15	92.7	82	75	74	69	6	5	92.6
10	114	125	99	15	26	82.8	139	57	68	53	4	15	84.8
11	150	171	135	15	36	84.1	162	100	112	97	3	15	91.5
12	94	105	91	3	14	91.5	163	46	53	46	0	7	92.9
13	150	166	145	5	21	91.8	235	63	68	59	4	9	90.1
14	105	113	100	5	13	91.7	236	63	78	61	2	17	86.5
15	61	78	61	0	17	87.8	239	65	66	58	7	8	88.5
16	94	103	95	0	8	96.4	240	52	62	48	4	14	84.2
17	83	94	83	0	11	93.8	255	129	147	123	6	24	89.1
18	75	85	72	3	13	90.0	291	26	31	26	0	5	91.2
19	86	117	84	2	33	82.8	319	19	19	19	0	0	100.0
20	61	64	60	1	4	96.0	324	33	33	33	0	0	100.0
Crossings													
	DRIVE dataset						STARE dataset						
ID	GT	Method	TP	FN	FP	F	ID	GT	Method	TP	FN	FP	F
1	26	25	20	6	5	78.4	1	13	15	12	1	3	85.7
2	27	28	22	5	6	80.0	2	17	13	13	4	0	86.7
3	30	30	28	2	2	93.3	3	10	9	9	1	0	94.7
4	21	20	17	4	3	82.9	4	7	7	7	0	0	100.0
5	27	28	23	4	5	83.6	5	16	19	15	1	4	85.7
6	38	39	32	6	7	83.1	44	12	12	11	1	1	91.7
7	24	25	22	2	3	89.8	77	19	17	17	2	0	94.4
8	21	19	16	5	3	80.0	81	25	26	23	2	3	90.2
9	23	24	21	2	3	89.4	82	21	23	19	2	4	86.4
10	26	29	22	4	7	80.0	139	21	17	15	6	2	79.0
11	39	38	31	8	7	80.5	162	41	36	34	7	2	88.3
12	26	29	25	1	4	90.9	163	21	17	17	4	0	89.5
13	26	27	22	4	5	83.0	235	22	21	19	3	2	88.4
14	22	23	19	3	4	84.4	236	27	23	21	6	2	84.0
15	15	14	14	1	0	96.5	239	28	29	27	1	2	94.7
16	35	33	32	3	1	94.1	240	18	16	15	3	1	88.2
17	20	18	18	2	0	94.7	255	29	27	25	4	2	89.3
18	25	20	19	6	1	84.4	291	7	6	6	1	0	92.3
19	24	25	23	1	2	93.9	319	9	9	9	0	0	100.0
20	25	24	24	1	0	98.0	324	7	7	7	0	0	100.0

REFERENCES

[1] Fathi A, Naghsh-Nilchi AR, Mohammadi FA (2013). Automatic vessel network features quantification using local vessel pattern operator. Comput. Biol. Med. 43:587–593.

[2] Al-Diri B, Hunter A, Steel D, Habib M (2010). Automated analysis of retinal vascular network connectivity. Comput. Med. Imaging Grap. 34(6):462–470.

[3] Calvo D, Ortega M, Penedo M, Rouco J (2011). Automatic detection and characterisation of retinal vessel tree bifurcations and crossovers in eye fundus images. Comput. Meth. Programs Biomed. 103:28–38.

[4] Azzopardi G, Petkov N (2011). Detection of Retinal Vascular Bifurcations by Trainable V4-Like Filters. LNCS. 6854:451–459.

[5] Lin KS, Tsai CL, Tsai CH, Sofka M, Chen SJ, Lin WY (2012). Retinal Vascular Tree Reconstruction With Anatomical Realism. IEEE T Bio-Med Eng. 59(12):3337–3347.

[6] Aibinu AM, Iqbal MI, Shafie AA, Salami MJE, Nilsson M (2010). Vascular intersection detection in retina fundus images using a new hybrid approach. Comput. Biol. Med. 40(1):81–89.

[7] Dashtbozorg B, Mendonca AM, Campilho A (2013). An Automatic Graph-based Approach for Artery/Vein Classification in Retinal Images. IEEE T. Image Process.

[8] Lupaşcu CA, Tegolo D, Trucco E (2010). FABC: Retinal vessel segmentation using AdaBoost. IEEE T Inf Technol B. 14:1267–1274.

[9] Lupaşcu CA, Tegolo D (2011). Stable automatic unsupervised segmentation of retinal vessels using self-organizing maps and a modified Fuzzy C-Means clustering. LNAI. 6857:244–252.

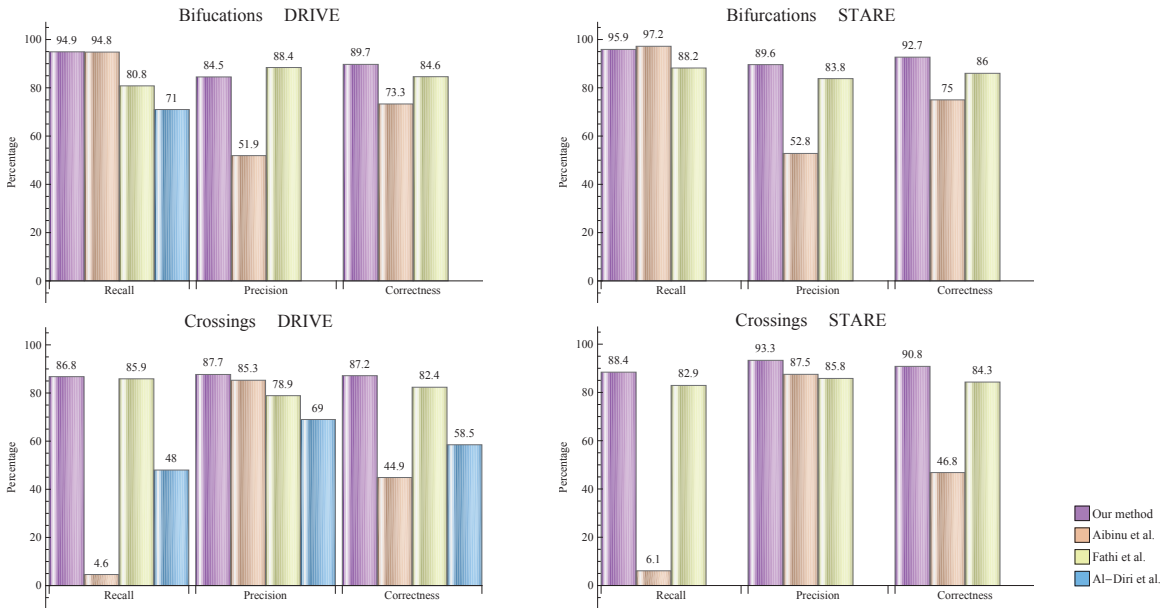

Fig. 5. Results comparison among our method and state-of-the-art algorithms. Missing data were not presented by their corresponding authors.

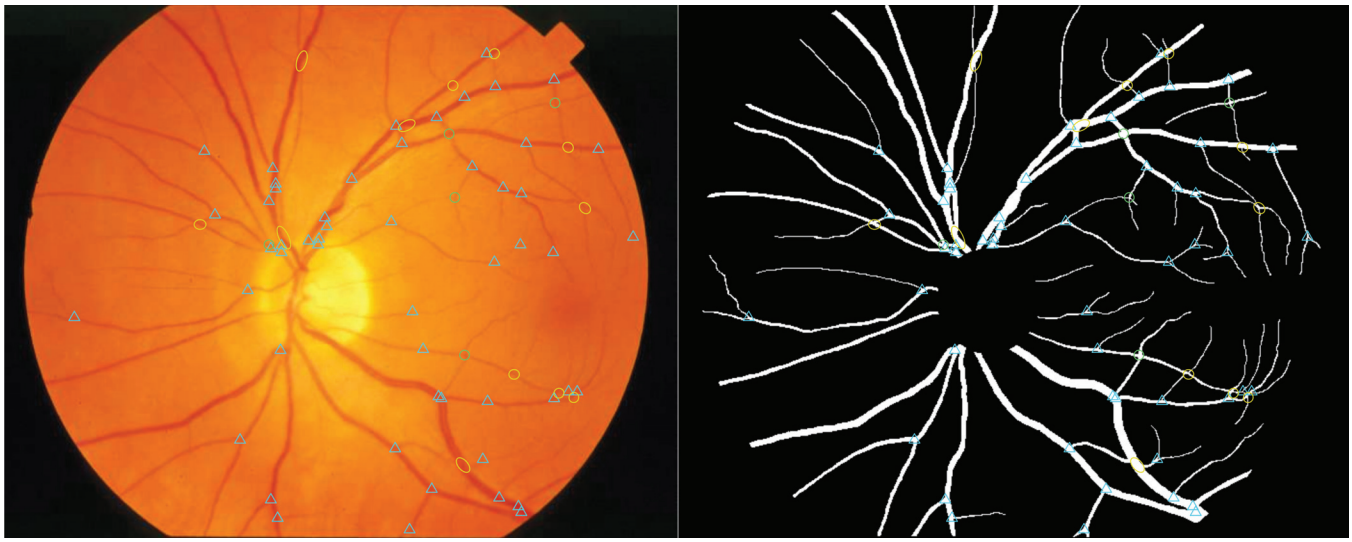

Fig. 6. Landmarks classification (bifurcations: blue triangles; direct crossings: green circles; non-direct crossings: yellow ellipsis) superimposed on image 163 from the STARE dataset, highlighted in Table I.

[10] Niemeijer M, Staal J, Ginneken B, Loog M, Abramoff MD (2004). Comparative study of retinal vessel segmentation methods on a new publicly available database. Proc. SPIE. 5370:648–656.

[11] Hoover A, Kouznetsova V, Goldbaum M (2000). Locating blood vessels in retinal images by piecewise threshold probing of a matched filter response. IEEE Trans. Med. Imaging. 19(3):203–210.

[12] Bhuiyan A, Nath B, Chua J, Ramamohanarao K (2007). Automatic Detection of Vascular Bifurcations and Crossovers from Color Retinal Fundus Images. Third Int'l IEEE Conference on SITIS. 711–718.

[13] Lam L, Lee S, Suen C (1992). Thinning methodologies: a comprehensive survey. IEEE Trans. Pattern Anal. Mach. Intell. 14(9):869–885.

[14] Lupaşcu CA, Tegolo D, Bellavia F, Valenti C (2013). Semi-automatic registration of retinal images based on line matching approach. International Symposium on CBMS, IEEE. 453–456.

[15] Lupaşcu CA, Tegolo D, Trucco E (2013). Accurate estimation of retinal vessel width using bagged decision trees and an extended multiresolution Hermite model. Med. Image Anal. 17(8):1164–1180.

[16] Niemeijer M, Xiayu X, Dumitrescu AV, Gupta P, Ginneken Bvan, Folk JC, Abramoff MD (2011). Automated Measurement of the Arteriolar-to-Venular Width Ratio in Digital Color Fundus Photographs. IEEE Trans. Med. Imaging. 30(11):1941–1950.

[17] Hatanaka Y, Muramatsu C, Hara T, Fujita H (2011). Automatic arteriovenous crossing phenomenon detection on retinal fundus images. Proc. SPIE, Medical Imaging: Computer-Aided Diagnosis. 7963.

[18] Bellavia F, Tegolo D, Valenti C (2011). Improving Harris corner selection strategy. IET Computer Vision 5(2):8796.

[19] Dehghani A, Moin MS, Saghafi M (2012). Localization of the optic disc center in retinal images based on the Harris corner detector. Biomed Eng Lett 2:198206.

[20] Bellavia F, Tegolo D, Valenti C (2014). Keypoint descriptor matching with context-based orientation estimation. Image and Vision Computing. http://dx.doi.org/10.1016/j.imavis.2014.05.002

[21] Bellavia F, Cacioppo A, Lupaşcu CA, Messina P, Scardina G, Tegolo D, Valenti C (2014). A non-parametric segmentation methodology for oral videocapillaroscopic images. Computer Methods and Programs in Biomedicine 114:240–246.

[22] Mirsharif Q, Tajeripour F (2012). Investigating image enhancement methods for better classification of retinal blood vessels into arteries and veins. International Symposium on AISP. 591–597.

[23] http://www5.cs.fau.de/research/data/fundus-images